Magnetization Reversal in Radially Distributed Nanowire Arrays

SCHOLARONE™
Manuscripts

Magnetization Reversal in Radially Distributed Nanowire Arrays

C. Garcia,[1, 2, *] W. O. Rosa,[3, 4] J. Garcia,[5, 6] V. M. Prida,[5] B. Hernando,[5] J. A. López,[1] P. Vargas,[1, 7] and C. A. Ross[8]

[1]*Departamento de Física, Universidad Técnica Federico Santa María,*
Avenida España 1680, 2390123 Valparaíso, Chile
[2]*Centro Científico y Tecnológico de Valparaiso, CCTVal, Valparaiso, Chile*
[3]*Dpto.de Física Aplicada, Universidad de Granada, C/Fuentenueva s/n, 18071, Granada, Spain*
[4]*Centro Brasileiro de Pesquisas Físicas, R. Dr. Xavier Sigaud, 150, 22290-180, Rio de Janeiro, Brazil*
[5]*Dpto. Física, Universidad de Oviedo, C/Federico García Lorca 18, 33007-Oviedo, Asturias, Spain*
[6]*IFW Dresden, Institute for Metallic Materials, P.O. Box 270116, D-01171 Dresden, Germany*
[7]*Centro para el Desarrollo de la Nanociencia y la Nanotecnología CEDENNA, Santiago, Chile*
[8]*Department of Materials Science and Engineering,*
Massachusetts Institute of Technology, Cambridge, Massachusetts 02139, USA
(Dated: February 7, 2018)

Abstract: The magnetic properties of radially-oriented Co, Ni, and CoNi alloy nanowires synthesized by pulsed electrodeposition into porous alumina structures are measured and compared with those of similar nanowires grown in a planar geometry. The alloy composition affects the anisotropy axis direction, which is determined by the balance between the magnetocrystalline and shape anisotropies, lying transverse to the nanowires for Co samples and along the nanowire axis for Ni. Monte Carlo simulations were performed to model the magnetic hysteresis of the radially-oriented and planar geometry nanowires using an approach based on a conical distribution of anisotropies. The model provides an excellent fit compared with experimental hysteresis loops.

INTRODUCTION

Nanoporous anodic alumina membranes (NAAMs), obtained through a double anodization process applied to aluminium, provide a particularly attractive self-assembled system which can be used as a template to fabricate other nanostructures. The anodic film contains a hexagonal array of parallel pores with pore size from 20 to 200 nm and interpore distance ranging from 60 to 500 nm, controlled via the anodization and subsequent etch conditions. Furthermore the pore locations can be templated by substrate patterning. The wide range of geometrical dimensions and the relatively simple electrochemical process involved in their fabrication make NAAMs very attractive for commercial biomedical ultramicrofiltration as well as for templates and masks for non-traditional lithographic methods,[1–5] for waveguides,[6] filters,[7] or magnetic recording media.[8] In addition, NAAMs can be suitably functionalized to be used in different sensing devices, or filled by electroplating[8,9] to grow densely packed long-range-ordered arrays of nanowires,[10] nanoparticles,[11] and nanotubes.[12]

Arrays of nanowires (NWs) made within planar nanoporous anodic alumina membranes (PNAAMs) have received particular attention due to their simple geometry, low fabrication cost, and possible device applications.[13] PNAAMs have been extensively used for the fabrication of magnetic nanowires with many different compositions [14–16] since the first work of Masuda and Fukuda.[9] NWs have shown a great potential for field

emission devices[17–20] and pH, bio-, and gas sensors,[21–24] as well as for their application as microwave devices[25–30] such as unbiased absorbers,[31] nonreciprocal isolators,[25] noise suppressors,[32,33] and circulators.[34]

The PNAAMs in these studies are typically prepared using an Al foil with planar geometry. More recently, it has also been proposed a cylindrical nanoporous anodic alumina membrane (CNAAM) geometry formed from an Al wire.[35–38] Previous related works carried out by Sanz et al. reported on the fabrication and magnetic characterization of electrodeposited Ni and Co nanowire arrays embedded in cylindrical and planar nanoporous anodic alumina templates,[35–37] and continuous $Ni_{80}Fe_{20}$ (Permalloy) cylindrical films and films with holes (antidots) made by replicating the close-packed pattern of the hexagonally arranged anodic alumina nanopores using sputter deposition.[36] The magnetic behaviour of the radially distributed Ni and Co nanowires was analyzed in terms of the effective magnetic anisotropy based on the geometry and magnetic properties of the wires, and further analysis of the magnetization reversal processes was performed by the First Order Reversal Curves (FORC) method.[38] Pang et al. demonstrated enhanced control over the growth and geometry of nanoporous alumina templates on non-planar surfaces of cylindrical and spherical Al patterns, relevant to applications where curved substrates are required, such as sensors, catalysts, and optic fibers[39]

In this work we have studied the effective anisotropy of magnetic nanowire arrays with different compositions that were synthesized by pulsed electrodeposition into the CNAAM templates. Depending on the composition the magnetic easy-axis direction and other magnetic properties can be controlled. The magnetic behavior in the transverse and axial directions are analyzed and com-

* carlos.garcia@usm.cl

pared with a micromagnetic model based on Monte Carlo simulation, where each magnetic nanowire in the array is modelled as a single magnetic moment or macrospin. The present study provides an experimental and theoretical description of the static properties of CNAAMs in order to facilitate applications including electromagnetic antenna devices[28] and filtration or separation technologies for microfluidics.[7]

EXPERIMENTAL PROCEDURE

High purity Al wires (Al 99.999 %, diameter = 1.5 mm, length = 15mm, Goodfellow) were selected to carry out the two-step anodization process.[9,15] Before the first anodization stage, the Al wires were electropolished for 2 minutes in a solution of perchloric acid and ethanol (25:75 vol%.). Then, the wires were anodized for 24 hours under a voltage of 40 V applied between the Al wire and a Pt counter-electrode mesh in 0.3 M oxalic acid electrolyte, kept at constant temperature of 4^0C. The non-uniform nanoporous alumina layer grown during the first anodization was removed by selective chemical etching in an aqueous solution of CrO_3 and H_3PO_4 for 10 hours. The second anodization process was then performed for 1 hour with the same electrochemical conditions, obtaining a 2.5 μm thick NAAM. The barrier layer thickness was reduced to around 4 nm by decreasing the applied voltage from 40 V down to 4.5 V.

Magnetic nanowire arrays with compositions Co_xNi_{1-x} ($x = 1, 0.75, 0$) were electrodeposited into the CNAAMs using pulsed electrodeposition. The resulting radially oriented nanowires had average diameters of 35 nm, interwire distance of 105 nm and 2.5 μm in length. In this work we kept the diameter and interpore distance constant and evaluated the influence of the composition of the wires. Cathodic deposition pulses of 8 ms in duration were applied under galvanostatic conditions at 38.2 mA/cm^2 for all the materials. Buffer salts, such as boric acid (H_3BO_3), were used to stabilize the electrolytes, maintaining a constant value of pH by reducing the effect of hydrogen evolution and inhibiting the formation of hydroxide species during the electrodeposition process. The pH of the electrolytes was adjusted to 4-4.5 with the addition of 1M dilute sodium hydroxide (NaOH) to the solution, and the electrochemical depositions were carried out in the temperature range between 45^0C and 65^0C, without mechanical stirring, in order to avoid precipitation of the boric acid.[16,40,41] The composition of the electrolytes and their working temperatures are detailed in Table 1.

Ferromagnetic nanowire arrays made of Co_xNi_{1-x} alloy were also pulse-electrodeposited in PNAAMs synthesized under similar conditions, as reported elsewhere [15]. The lattice parameters of the nanowires synthesized in the PNAAMs templates, namely the diameter, interwire distance and length are the same as those of the CNAAMs, in order to allow for a direct comparison.

TABLE 1. Electrolytes and conditions employed for the electrodeposition of pure Co and Ni nanowires and $Co_{75}Ni_{25}$ alloyed nanowires.

Salts	Co (g/l)	Ni (g/l)	$Co_{75}Ni_{25}$ (g/l)
$CoSO_4 \cdot 7H_2O$	300	–	150
$NiSO_4 \cdot 6H_2O$	–	300	150
$CoCl_2 \cdot 6H_2O$	45	–	22.5
$NiCl_2 \cdot 6H_2O$	–	45	22.5
H_3BO_3	45	45	45
pH	4	4	4
Temperature (°C)	65	45	65

Morphological characterization was performed by high resolution scanning electron microscopy in an FEI XL30 FEG-ESEM. Fig. 1.a shows SEM images of a typical substrate consisting of the Al wire after the second anodization step, and Fig. 1.b-d show the sample after electrodeposition of Ni nanowires within the nanopores of the alumina template. Locally the structure resembles a PNAAM because the curvature is small compared to the oxide thickness, and the electrodeposition of magnetic material into the pores showed the same efficiency found in NAAMs. The alumina nanopores displayed in the Fig. 1.c are arranged in hexagonally close-packed grains or domains with different lattice orientations that extend over several square micrometers, covering the whole surface of the Al wire substrate.
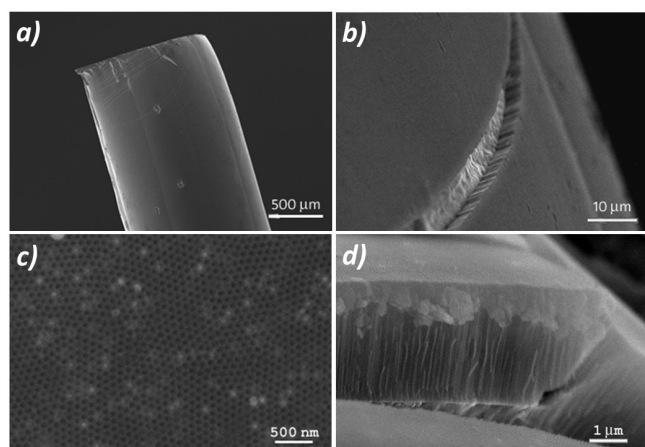

FIG. 1. HRSEM images of the Ni nanowire arrays electrochemically grown in the CNAAM structure; (a) Substrate consisting of the Al wire after the second anodization step, (b) cross-section of the nanoporous anodic alumina layer grown on the surface of the Al wire substrate, (c) top-view of the electrodeposited Ni nanowires grown inside the hexagonally ordered pores of the CNAAM template and (d) higher magnification cross section image of the electrodeposited Ni nanowires embedded in the parallel aligned channels of the nanoporous alumina template.

A schematic drawing of the cylindrical distribution of the magnetic nanowires and directions of the applied magnetic field is shown in Figure 2. Magnetic hystere-

sis loops were measured at room temperature in two directions, axial and transverse with respect to the Al wire axis, using a vibrating sample magnetometer (ADE model 1660) up to a maximum external applied field of 10 kOe.
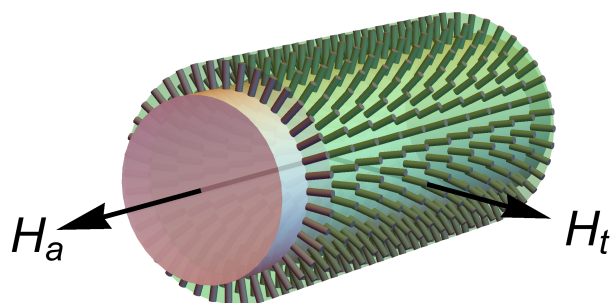

FIG. 2. Schematic transverse view of the CNAAM filled with nanowires. Axial and transverse directions of the applied magnetic field are displayed.

THEORETICAL MODEL BASED ON MONTE CARLO SIMULATIONS

Each sample has a 1.5 mm diameter and 50 mm length, and therefore contains 4.9×10^5 nanowires around its circumference and 7×10^{11} wires in total. This number is too large to be simulated. In the spirit of the fast Monte Carlo (MC) approach,[42] we scale down the system to enable micromagnetic simulations. By considering 12 nanowires per circle, there are 242 nanowires in total to maintain a diameter/length ratio equal to that of the experimental sample, so the MC model has a reduced diameter of 330 nm and a length of 2.5 μm. Each nanowire is modeled as a single magnetic moment (a macrospin). To estimate the size of the macrospin, m, in this scaled Monte Carlo simulation we use the experimental result that the sample is almost saturated at room temperature for an external field of about 10 kOe, and fit this to a Langevin function to determine the magnetic moment. These considerations yield a magnetization $m = 10^4 \mu_B$ for Ni and $m = 3 \times 10^4 \mu_B$ for Co in the scaled wires. The magnitude of the dipolar interaction energy between nanowires (spacing 90 nm) is estimated as being on the order of 0.1 meV for Ni and 1 meV for Co, giving an interaction field of 1.7 Oe and 17 Oe for Ni and Co nanowires respectively. Consequently the dipole-dipole interaction is weak in these systems compared to other energy terms, especially in the arrays of Ni NWs.

The macroscopic hysteresis was modelled by considering a collection of macrospins with Zeeman energy, an effective anisotropy and the weak dipole dipole interaction. Each macrospin corresponds to a single nanowire. To account for variation in the direction of the nanowires' magnetic anisotropy, the anisotropy axis of each wire lies on the surface of a cone oriented radially outwards from the Al wire which is characterized by its interior cone angle (Fig. 3). The cone angle has a uniform distribution with mean α and width σ_α to capture the dispersion in the direction of the anisotropy of the nanowires. In other words, each nanowire is represented by a macrospin with an anisotropy which is oriented at an angle with a dispersion given by $\alpha \pm \sigma_\alpha$. The anisotropy angle and its dispersion capture the effects of a spread in the c-axis orientation or other contributions to anisotropy[43–47].

The energy of the system, E, is a function of the micro state $\mu = \{\vec{m}_i\}$, i.e. the energy of all magnetic moments in thermodynamic equilibrium separated by distances r_{ij}, and it is given by

$$E = \sum_{i=1}^{N} -\frac{KV_i}{2}\left(\frac{\vec{m}_i}{m_i} \cdot \hat{n}_i\right)^2 - \sum_{i=1}^{N} \vec{m}_i \cdot \vec{H} \\ + \sum_{i>j} \frac{(\vec{m}_i \cdot \vec{m}_j - 3(m_i \cdot \hat{n}_{ij})(m_j \cdot \hat{n}_{ij}))}{r_{ij}^3} \quad (1)$$

where KV_i is the anisotropy constant times the volume of the i-th wire and includes both shape and magnetocrystalline anisotropy, N is the number of wires ($N = 400$) in the cylinder, $\hat{n}_i$ is the unit vector representing the anisotropy axis of the ith-wire, the vector $\vec{m}_i$ represents the effective magnetic moment of the ith wire, the vector $\vec{m}_j$ represents the effective magnetic moment of the jth wire, $\hat{n}_{ij}$ denotes a unit vector along the direction that connects the magnetic moments, r_{ij} represents the distance between ith and the jth wire, and $\vec{H}$ stands for the external magnetic field.
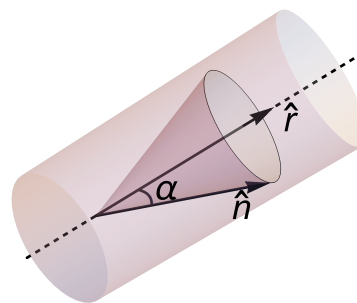

FIG. 3. Schematic drawing of the conical anisotropy distribution in a single nanowire.

The numerical simulations were performed by using the standard MC method together with the Metropolis algorithm[48] satisfying the detailed balance in which the probability of acceptance for a transition between two micro-states, $A(\mu \to \nu)$, is given by the following procedure:

$$A(\mu \to \nu) = \begin{cases} e^{-\beta \Delta E} & \Delta E > 0 \\ 1 & \Delta E \leq 1 \end{cases} \quad (2)$$

The simulation parameters are temperature T=300 K, and external magnetic field ranging from -12 kOe to

12 kOe. The values of effective magnetic moments vary between $3 \cdot 10^4$ and 10^4 Bohr magnetons for Co and Ni nanowires, respectively. Effective anisotropy values fall in the range of standard experimental values. The effective anisotropy constant times volume, KV, is $1.11 \cdot 10^{-16}$ Joule for nickel and $2.23 \cdot 10^{-16}$ Joule for cobalt.

The anisotropy axes of the wires are uniformly distributed with an average cone angle of α. In the case of nickel the average angle is $\alpha(\text{Ni}) = 2.5°$ with a width of the distribution of $2.5°$ whereas for cobalt the average value is $\alpha(\text{Co}) = 30°$ and the width is $5°$. These values were found by fitting the magnetization curves for different anisotropy angles with the model proposed in Eq. 1. In all cases, dipole-dipole interaction was taken into account. Therefore, the Ni easy anisotropy axis is close to the wire axis, whereas for Co (and also for CoNi) there is a tilted anisotropy direction. A tilted magnetocrystalline anisotropy axis has previously been reported in CoNi nanowires[43–47]. This gave a better fit than having the anisotropy direction along or across the wire axis. Hysteresis loops were modeled by the Monte Carlo method for the parameters detailed in Table 2.

TABLE 2. Model parameters of the magnetic systems.

Material	$M_S[\mu_B]$	KV $[10^{-16}$ J]	α	σ_α	T_{MC} [K]
Nickel	10000	1.1	2.5	2.5	300
$Co_{75}Ni_{25}$	25000	1.95	28	4	300
Cobalt	30000	2.23	30	5	300

RESULTS AND DISCUSSION

A. Magnetic hysteresis loops of CNAAM nanowires

Magnetic hysteresis loops of ferromagnetic nanowires arranged in cylindrical (CNAAM) samples with composition Co_xNi_{1-x} (x = 1, 0.75, 0), were measured for the applied magnetic field axial (along the axis of the Al wire) and transverse (along the radial direction) to the Al wire axis. A comparison between theoretical and experimental results for Ni, Co and CoNi NW arrays is shown in Fig. 4(a-f).

The coercive field, H_C, and normalized remanent magnetization, $m_r = \mathbf{M_r}/\mathbf{M_s}$, were obtained from the hysteresis loops. Table 3 summarizes both, H_C and m_r, for each composition of the NWs and applied field direction. Coercivities of 699 Oe and 167 Oe were obtained for Ni nanowires with transverse and axial magnetic field directions, with normalized remanence of 0.57 and 0.07, respectively. In contrast, Co nanowire arrays exhibit more isotropic behavior with coercivities of 1224 Oe and 929 Oe for the transverse and axial applied magnetic field, respectively. Co and $Co_{75}Ni_{25}$ NWs exhibit a very similar magnetic behaviour in terms of coercive field, remanence and angular dependence of coercivity.

Due to the peculiar geometrical distribution of

TABLE 3. Typical H_C and M_r values for magnetic nanowires with composition Co, CoNi, and Ni measured for axial and transverse magnetic field directions.

Material	$H_C^{\parallel}$	$M_r^{\parallel}$	$H_C^{\perp}$	$M_r^{\perp}$
Co	929	0.27	1224	0.44
$Co_{75}Ni_{25}$	788	0.26	1094	0.38
Ni	167	0.068	699	0.57

CNAAM nanowires, the transverse direction of the applied field measures a system with wires oriented at all angles to the applied magnetic field. In Co, the high remanence for the axial field is indicative of the contribution of the magnetocrystalline anisotropy orthogonal to the nanowires. Ni, on the other hand, has a well defined hard magnetization axis for the axial applied field, which is perpendicular to the Ni wire length.

The differences in magnetic properties found for the three NW compositions arise from their different magnetic anisotropy contributions. Shape anisotropy is significant for nanowires leading to an easy magnetization axis along the length of the nanowire. Magnetocrystalline anisotropy in Ni is weak and makes little contribution for a polycrystalline nanostructure,[49] but magnetocrystalline anisotropy is particularly important for Co nanowires that usually[50,51] crystallize with hcp structure in which the c-axis grows perpendicular to the nanowire length, giving rise to transverse domains. For the Co-rich nanowires, the hysteresis loops in the axial and transverse field directions are similar[52] because both average over a variety of nanowire easy magnetization axis orientations.

The competition between magnetic anisotropies in these nanowire arrays is also shared by nanowire arrays within planar anodic alumina templates, although in the CNAAM samples a novel magnetic response is observed due to the special feature of cylindrical geometry. Fig. 4 compares CNAAM and PNAAM NWs hysteresis loops. For PNAAM NW samples, out-of-plane refers to a magnetic field applied out of the film plane, along the nanowires axis, while in-plane refers to a field applied in the plane of sample, therefore transverse to the nanowires axis. The PNAAM in-plane loops and CNAAM axial loops are expected to be similar because they represent measurements orthogonal to all the nanowires in the array. However, the PNAAM out-of-plane loops and CNAAM transverse loops differ because the nanowires in the CNAAM case are oriented at a range of angles with respect to the field, giving lower remanence values.

B. Angular dependence of magnetic hysteresis

As different magnetization reversal mechanisms would give a different angular dependence of the coercivity H_C, the measurements of $H_C(\theta)$ provide helpful information about the magnetization reversal mechanisms in arrays of ferromagnetic nanowires.

The angular dependence of remanence and coercive field has been previously studied[53–56] in nanowire ar-
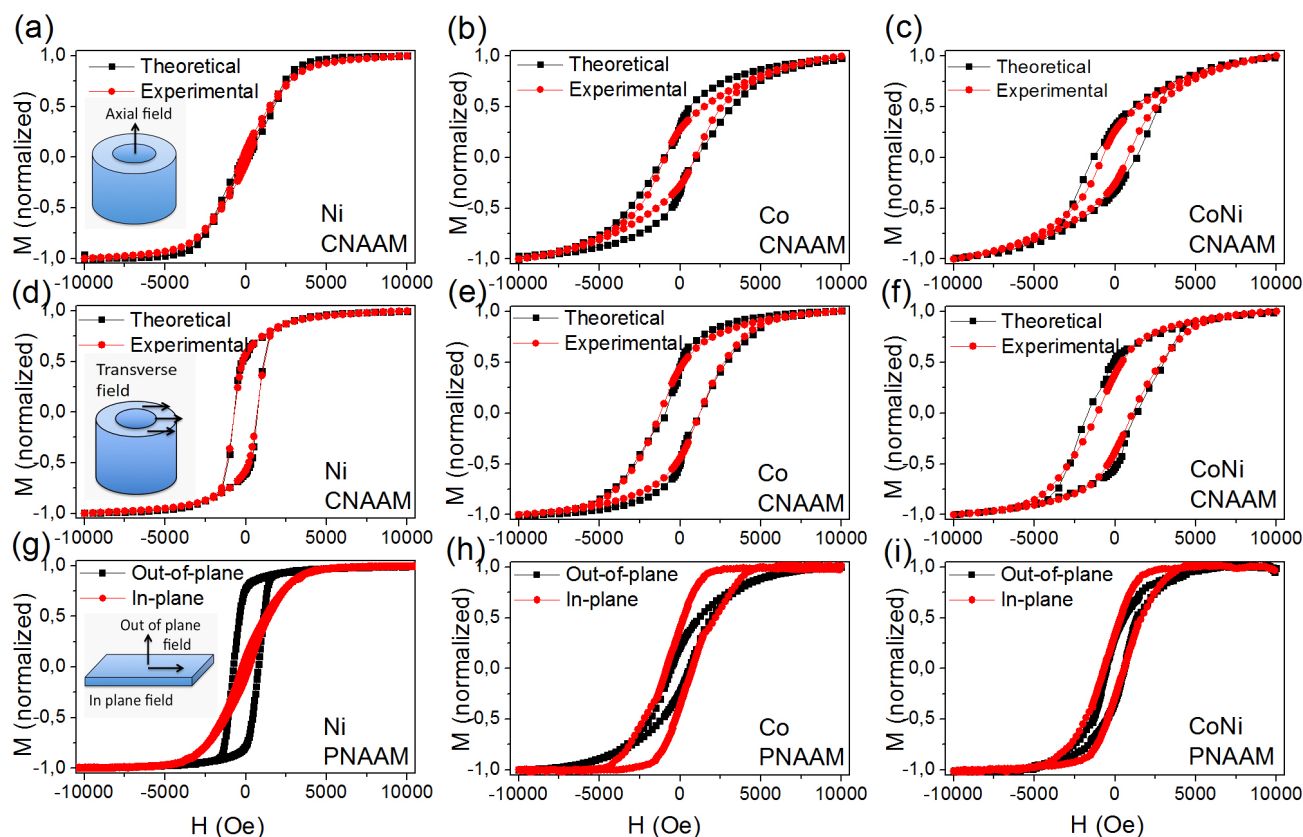
FIG. 4. Experimental and MC model hysteresis loops for Ni (a, d), Co (b, e) and CoNi (c, f) nanowires in a CNAAM with magnetic field applied axial and transverse with respect to the Al wire. The model used the values given in Table II. Hysteresis loops for in-plane (PNAAM) nanowires with compositions (g) Ni, (h) Co and (i) $Co_{75}Ni_{25}$.

rays made from Co, Ni, CoNi, NiFe and CoNiFe alloy compositions. However, a consistent theoretical model is still lacking, particularly for materials having mixed anisotropies as in the case of the Co NWs studied here. Lavin et al. developed analytical models of the angular dependence of coercivity for Ni nanowire arrays, showing that the wires reverse their magnetization by the propagation of a transverse domain wall.[54] The two other mechanisms of magnetization reversal (coherent magnetization reversal and the curling mode) have been shown to require higher energy.

For Co nanowire arrays, it is well-known that the high magnetocrystalline anisotropy can influence the easy magnetization axis direction. Lavin et al.[55] compared experimental and micromagnetic results for a single Co nanowire and an array of Co magnetic nanowires. This showed a maximum of the coercivity when the angle between the applied field and the long axis of the wire is about 60°. This behavior was interpreted as an effect of dipolar interactions among Co nanowires, but as we show in Figure 5, our model of non-interacting nanowires with a conical anisotropy distribution as given in Table 2, is able to reproduce the angular distribution of coercive field in nanowire arrays.

Studies of the angular dependence of the magnetization

reversal of CNAAM NW samples were also performed, in which the hysteresis loop was measured for different angles between the axis of the aluminum wire and the external magnetic field. Fig. 5a and b show the polar representation of the coercive field angular dependence for Co and Ni samples, respectively. The polar representation for $Co_{75}Ni_{25}$ NWs is not shown because is almost identical to that of the Co sample. The angular dependence of the magnetization reversal was compared with the result based on the Monte Carlo model. Fig. 5c shows the excellent fitting of the angular dependence of coercive field for the Co and Ni models using parameters of Table 2. The error bars shown in the Monte Carlo results correspond to the standard deviation of ten simulated hysteresis loops, each of them computed with a random seed. The observed larger standard deviation of the angular dependence of coercivity of cobalt nanowires, when compared with the Ni sample, can be attributed to a larger spread in the anisotropy cone angle, which increases the misalignment at zero field. The error bars for the experimental results are hidden by the symbol size. The match between the micromagnetic model and the experimental results is excellent.

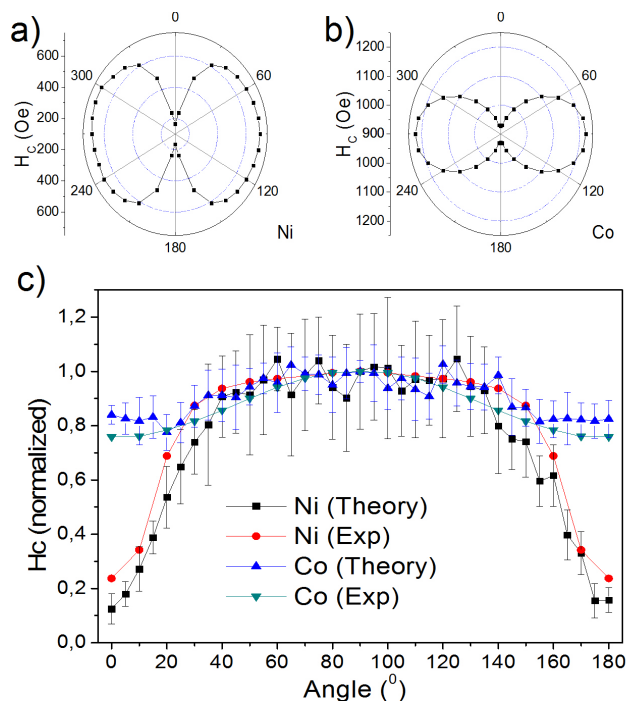The hysteresis of the Ni NW arrays is therefore well described by a model of weak interacting NWs with

FIG. 5. Angular dependence of the coercivity of nanowires grown in a CNAAM with composition (a) Ni, (b) Co, shown in polar representation. (c) Experimental and Monte Carlo modeling results for the angular dependence of the coercive field of Co and Ni nanowire arrays in CNAAMs.

the direction of the easy magnetization axis lying close to the NW axis, as expected from the dominant shape anisotropy. However, the Co (and CoNi) wires show better fits for a tilted anisotropy. This cannot arise from the sum of two orthogonal anisotropies (shape and magnetocrystalline anisotropy, if the Co c-axis is perpendicular to the NW length), and it may indicate a spread in c-axis orientation or another contribution to anisotropy.[43,44,46,47] The discrepancies between our model and the experimental data are probably due to the limitation of the macrospin approximation to model incoherent reversal, using a macrospin with anisotropy for each nanowire, which probably occurs in Co and CoNi nanowires. For this reason the model provides an excellent fitting for Ni nanowires, but it does not work as satisfactorily in the case of Co-rich wires.

CONCLUSIONS

Arrays of Ni, Co and CoNi alloy nanowires were prepared by template-assisted electrochemical deposition in porous anodic alumina membranes with both cylindrical and planar geometry. Monte Carlo simulations of a set of weak interacting macrospins with appropriate orientations were used to model the magnetic hysteresis loops of the nanowires, as well as the angular dependence of the coercive field, by considering a conical distribution

of easy anisotropy axes. The main result is that the MC model reproduces both the hysteresis loops and the angular dependence of coercive field very well. This approach will be useful for designing magnetic devices based on ferromagnetic nanowires arranged in cylindrical geometries.
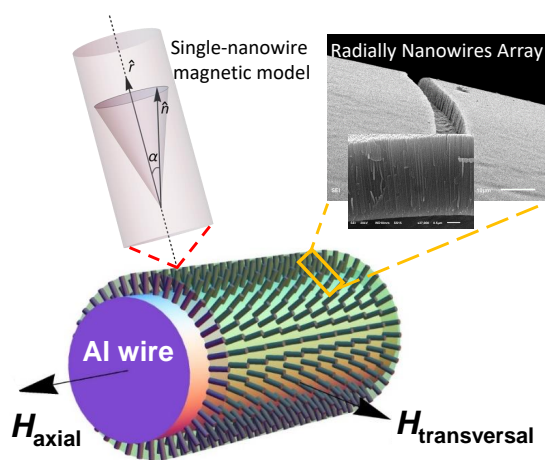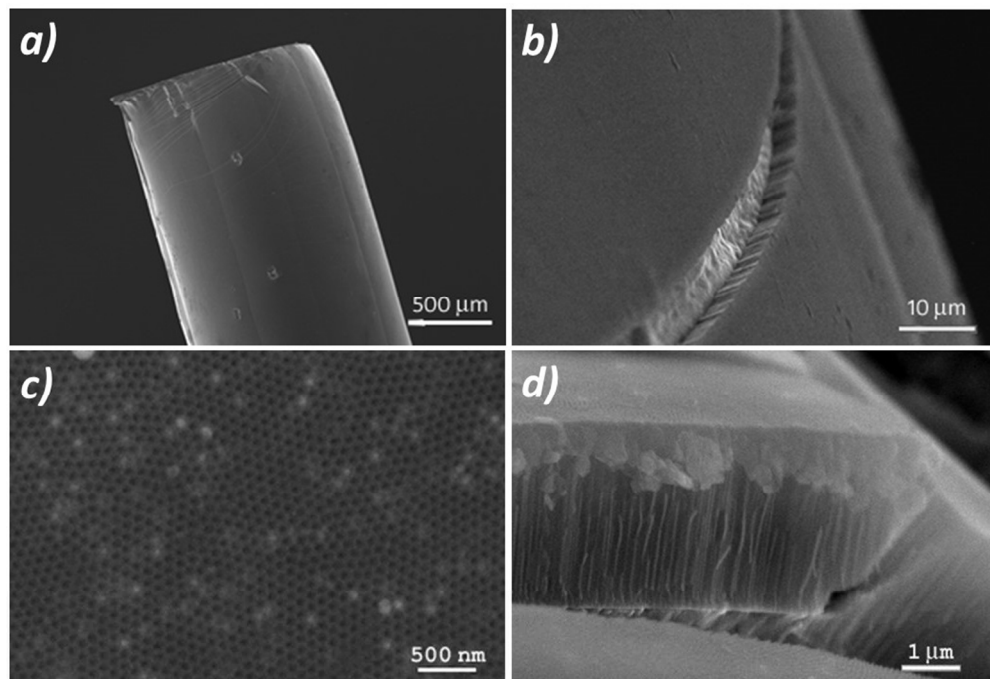
References

(1) Razpet, A.; Johansson, A.; Possnert, G.; Skupiski, M.; Hjort, K.; Halln, A. Fabrication of High-Density Ordered Nanoarrays in Silicon Dioxide by MeV Ion Track Lithography. *J. Appl. Phys.* **2005**, *97*, 044310.

(2) Nakao, M.; Oku, S.; Tamamura, T.; Yasui, K.; Masuda, H. GaAs and InP Nanohole Arrays Fabricated by Reactive Beam Etching Using Highly Ordered Alumina Membranes. *Japanese J. Appl. Phys.* **1999**, *38*, 1052.

(3) Almawlawi, D.; Bosnick, K. A.; Osika, A.; Moskovits, M. Fabrication of Nanometer-Scale Patterns by Ion-Milling with Porous Anodic Alumina Masks. *Adv. Mater.* **2000**, *12*, 1252–1257.

(4) Matsuura, N.; Simpson, T. W.; Mitchell, I. V.; Mei, X.-Y.; Morales, P.; Ruda, H. E. Ultrahigh-Density, Non-lithographic, sub-100 nm Pattern Transfer by Ion Implantation and Selective Chemical Etching. *Appl. Phys. Lett.* **2002**, *81*, 4826–4828.

(5) Sanz, R.; Johansson, A.; Skupinski, M.; Jensen, J.; Possnert, G.; Boman, M.; Vazquez, M.; Hjort, K. Fabrication of Well-Ordered High-Aspect-Ratio Nanopore Arrays in TiO2 Single Crystals. *Nano Lett.* **2006**, *6*, 1065–1068.

(6) Jamois, C.; Wehrspohn, R.; Andreani, L.; Hermann, C.; Hess, O.; Gsele, U. Silicon-Based Two-Dimensional Photonic Crystal Waveguides. *Phot. Nano. Fund. Appl.* **2003**, *1*, 1 – 13.

(7) Berthier, J.; Rivera, F.; Caillat, P.; Berger, F. Dimensioning of a New Micro-Needle for the Dispense of Drugs in Tumors and Cell Clusters. *Nanotech 2005, Technical Proceedings of the 2005 NSTI Nanotechnology Conference and Trade Show* **2005**, *1*, 652–655.

(8) Shingubara, S. Fabrication of Nanomaterials Using Porous Alumina Templates. *J. Nanopart. Res. 5*, 17–30.

(9) Masuda, H.; Fukuda, K. Ordered Metal Nanohole Arrays Made by a Two Step Replication of Honeycomb Structures of Anodic Alumina. *Science* **1995**, *268*, 1466–1468.

(10) Vazquez, M.; Pirota, K.; Hernandez-Velez, M.; Prida, V. M.; Navas, D.; Sanz, R.; Batalln, F.; Velazquez, J. Magnetic Properties of Densely Packed Arrays of Ni Nanowires as a Function of Their Diameter and Lattice Parameter. *J. Appl. Phys.* **2004**, *95*, 6642–6644.

(11) Hernández-Vélez, M.; Pirota, K.; Pászti, F.; Navas, D.; Climent, A.; Vázquez, M. Magnetic Nanowire Arrays in Anodic Alumina Membranes: Rutherford Backscattering Characterization. *Appl. Phys. A* **2005**, *80*, 1701–1706.

(12) Johansson, A.; Trndahl, T.; Ottosson, L.; Boman, M.; Carlsson, J.-O. Copper Nanoparticles Deposited Inside the Pores of Anodized Aluminium Oxide Using Atomic Layer Deposition. *Mater. Sci. Eng. C* **2003**, *23*, 823 – 826.

(13) Piraux, L.; Encinas, A.; Vila, L.; Mtfi-Tempfli, S.; Mtfi-Tempfli, M.; Darques, M.; Elhoussine, F.; Michotte, S. Magnetic and Superconducting Nanowires. *J. Nanosci. Nanotechnol.* **2005**, *5*, 372–389.

(14) Jessensky, O.; Mller, F.; Gsele, U. Self-Organized Formation of Hexagonal Pore Arrays in Anodic Alumina. *Appl. Phys. Lett.* **1998**, *72*.

(15) Prida, V. M.; Vega, V.; Garcia, J.; Iglesias, L.; Hernando, B.; Minguez-Bacho, I. Electrochemical Methods for Template-Assisted Synthesis of Nanostructured Materials, in Magnetic Nano- and Microwires: Design, Synthesis, Properties and Applications Part I: Design and Synthesis of Magnetic Nano- and Microwires. *Woodhead Publishing Series in Electronic and Optical Materials (Elsevier)* **2015**, *268*, 3–39.

(16) Prida, V. M.; Garcia, J.; Hernando, B.; Bran, C.; Vivas, L. G.; Vazquez, M. Electrochemical Synthesis of Magnetic Nanowires with Controlled Geometry and Magnetic Anisotropy, in Magnetic Nano- and Microwires: Design, Synthesis, Properties and Applications Part I: Design and Synthesis of Magnetic Nano- and Microwires. *Woodhead Publishing (Elsevier)* **2015**, *268*, 41–104.

(17) Vila, L.; Vincent, P.; Dauginet-De Pra, L.; Pirio, G.; Minoux, E.; Gangloff, L.; Demoustier-Champagne, S.; Sarazin, N.; Ferain, E.; Legras, R. *et al.* Growth and Field-Emission Properties of Vertically Aligned Cobalt Nanowire Arrays. *Nano Lett.* **2004**, *4*, 521–524.

(18) Dangwal, A.; Pandey, C. S.; Mller, G.; Karim, S.; Cornelius, T. W.; Trautmann, C. Field Emission Properties of Electrochemically Deposited Gold Nanowires. *Appl. Phys. Lett.* **2008**, *92*.

(19) Navitski, A.,; Mller, G.,; Sakharuk, V.,; Cornelius, T. W.,; Trautmann, C.,; Karim, S., Efficient Field Emission From Structured Gold Nanowire Cathodes. *Eur. Phys. J. Appl. Phys.* **2009**, *48*, 30502.

(20) Baranova, L.; Baryshev, S.; Gusinskii, G.; Konnikov, S.; Nashchekin, A. Nickel field-emission microcathode: Art of fabrication, properties, and applications. *Nuclear Instruments and Methods in Physics Research Section B: Beam Interactions with Materials and Atoms* **2010**, *268*, 1686 – 1688.

(21) Antohe, V. A.; Radu, A.; Mtfi-Tempfli, M.; Attout, A.; Yunus, S.; Bertrand, P.; Duu, C. A.; Vlad, A.; Melinte, S.; Mtfi-Tempfli, S. *et al.* Nanowire-Templated

Microelectrodes for High-Sensitivity pH Detection. *Appl. Phys. Lett.* **2009**, *94*.

(22) Shi, A. W.; Qu, F. L.; Yang, M. H.; Shen, G. L.; Yu, R. Q. Amperometric {H2O2} Biosensor Based on Poly-Thionine Nanowire/HRP/nano-Au-Modified Glassy Carbon Electrode. *Sens. Actuators, B* **2008**, *129*, 779 – 783.

(23) Walter, E. C.; Penner, R. M.; Liu, H.; Ng, K. H.; Zach, M. P.; Favier, F. Sensors From Electrodeposited Metal Nanowires. *Surf. Interface Anal.* **2002**, *34*, 409–412.

(24) Aravamudhan, S.; Kumar, A.; Mohapatra, S.; Bhansali, S. Sensitive Estimation of Total Cholesterol in Blood Using Au Nanowires Based Micro-Fluidic Platform. *Biosens. Bioelectron.* **2007**, *22*, 2289 – 2294.

(25) Kuanr, B. K.; Veerakumar, V.; Marson, R.; Mishra, S. R.; Camley, R. E.; Celinski, Z. Non-reciprocal Microwave Devices Based on Magnetic Nanowires. *Appl. Phys. Lett.* **2009**, *94*.

(26) Darques, M.; la Torre Medina, J. D.; Piraux, L.; Cagnon, L.; Huynen, I. Microwave Circulator Based on Ferromagnetic Nanowires in an Alumina Template. *Nanotechnology* **2010**, *21*, 145208.

(27) De La Torre Medina, J.; Spiegel, J.; Darques, M.; Piraux, L.; Huynen, I. Differential Phase Shift in Nonreciprocal Microstrip Lines on Magnetic Nanowired Substrates. *Appl. Phys. Lett.* **2010**, *96*.

(28) Saib, A.; Vanhoenacker-Janvier, D.; Huynen, I.; Encinas, A.; Piraux, L.; Ferain, E.; Legras, R. Magnetic Photonic Band-Gap Material at Microwave Frequencies Based on Ferromagnetic Nanowires. *Appl. Phys. Lett.* **2003**, *83*.

(29) Allaeys, J.-F.; Marcilhac, B.; Mage, J.-C. Influence of Track-Etching on Polycarbonate Membrane Permittivity. *J. Phys. D: Appl. Phys.* **2007**, *40*, 3714.

(30) Boucher, V.; Ménard, D. Effective Magnetic Properties of Arrays of Interacting Ferromagnetic Wires Exhibiting Gyromagnetic Anisotropy and Retardation Effects. *Phys. Rev. B* **2010**, *81*, 174404.

(31) Encinas, A.; Demand, M.; Vila, L.; Piraux, L.; Huynen, I. Tunable Remanent State Resonance Frequency in Arrays of Magnetic Nanowires. *Appl. Phys. Lett.* **2002**, *81*.

(32) Kuanr, B. K.; Marson, R.; Mishra, S. R.; Kuanr, A. V.; Camley, R. E.; Celinski, Z. J. Gigahertz Frequency Tunable Noise Suppressor Using Nickel Nanorod Arrays and Permalloy Films. *J. Appl. Phys.* **2009**, *105*.

(33) Nam, B.; Choa, Y.-H.; Oh, S.-T.; Lee, S. K.; Kim, K. H. Broadband RF Noise Suppression by Magnetic Nanowire-Filled Composite Films. *Magnetics, IEEE Transactions on* **2009**, *45*, 2777–2780.

(34) Saib, A.; Darques, M.; Piraux, L.; Vanhoenacker-Janvier, D.; Huynen, I. Unbiased Microwave Circulator Based on Ferromagnetic Nanowires Arrays of Tunable Magnetization State. *J. Phys. D: Appl. Phys.* **2005**, *38*, 2759.

(35) Sanz, R.; Hernandez-Velez, M.; Pirota, K.; Baldonedo, J. L.; Vazquez, M. Fabrication and Magnetic Functionalization of Cylindrical Porous Anodic Alumina. *Small* **2007**, *3*, 434–437.

(36) Sanz, R.; Navas, D.; Vazquez, M.; Hernandez-Velez, M.; Ross, C. A. Preparation and Magnetic Properties of Cylindrical NiFe Films and Antidot Arrays. *J. Nanosci. Nanotechnol.* **2010**, *10*, 6775–6778.

(37) Sanz, R.; Vazquez, M.; Pirota, K. R.; Hernandez-Velez, M. Radially Distributed Ni and Co Nanowire Arrays. *J. Appl. Phys.* **2007**, *101*.

(38) Garcia, J.; Prida, V.; Vega, V.; Rosa, W.; Caballero-Flores, R.; Iglesias, L.; Hernando, B. 2D and 3D Ordered Arrays of Co Magnetic Nanowires. *J. Magn. Magn. Mater.* **2015**, *383*, 88 – 93.

(39) Pang, Y.; Chandrasekar, R. Cylindrical and Spherical Membranes of Anodic Aluminum Oxide with Highly Ordered Conical Nanohole Arrays. *Natural Science* **2015**, *7*, 232 – 237.

(40) Nikolic, N. D.; Pavlovic, L. J.; Pavlovic, M. G.; Popov, K. I. Effect of Temperature on the Electrodeposition of Disperse Copper Deposits. *J. Serb. Chem. Soc.* **2007**, *72*.

(41) Santos, J.; Matos, R.; Trivinho-Strixino, F.; Pereira, E. Effect of Temperature on Co Electrodeposition in the Presence of Boric Acid. *Electrochim. Acta* **2007**, *53*, 644 – 649.

(42) Vargas, P.; Altbir, D.; d'Albuquerque e Castro, J. Fast Monte Carlo Method for Magnetic Nanoparticles. *Phys. Rev. B* **2006**, *73*, 092417.

(43) Diaz Barriga-Castro, E.; Garcia, J.; Mendoza-Resendez, R.; Prida, V. M.; Luna, C. Pseudo-Monocrystalline Properties of Cylindrical Nanowires Confinedly Grown by Electrodeposition in Nanoporous Alumina Templates. *RSC Adv.* **2017**, *7*, 13817–13826.

(44) Garcia, J.; Vega, V.; Iglesias, L.; Prida, V. M.; Hernando, B.; Barriga-Castro, E. D.; Mendoza-Resendez, R.; Luna, C.; Goerlitz, D.; Nielsch, K. Template-Assisted Co-Ni Alloys and Multisegmented Nanowires with Tuned Magnetic Anisotropy. *Phys. Status Solidi A* **2014**, *211*, 1041–1047.

(45) Vega, V.; Boehnert, T.; Martens, S.; Waleczek, M.; Montero-Moreno, J. M.; Goerlitz, D.; Prida, V. M.; Nielsch, K. Tuning the Magnetic Anisotropy of CoNi Nanowires: Comparison Between Single Nanowires and Nanowire Arrays in Hard-Anodic Aluminum Oxide Membranes. *Nanotechnology* **2012**, *23*, 465709.

(46) Samardak, A.; Ognev, A.; Samardak, A.; Stebliy, E.; Modin, E.; Chebotkevich, L.; Komogortsev, S.; Stancu, A.; Panahi-Danaei, E.; Fardi-Ilkhichy, A. *et al.* Variation of Magnetic Anisotropy and Temperature-Dependent FORC Probing of Compositionally Tuned Co-Ni Alloy Nanowires. *J. Alloys Compd.* **2018**, *732*, 683 – 693.

(47) Samardak, A.; Nasirpouri, F.; Nadi, M.; Sukovatitsina, E.; Ognev, A.; Chebotkevich, L.; Komogortsev, S. Conversion of Magnetic Anisotropy in Electrodeposited CoNi Alloy Nanowires. *J. Magn. Magn. Mater.* **2015**, *383*, 94 – 99, Selected papers from the sixth Moscow International Symposium on Magnetism (MISM-2014).

(48) Binder, K.; Heermann, D. W. Monte Carlo Simulation in Statistical Physics. **2010**,

(49) Skomski, R.; Zeng, H.; Zheng, M.; Sellmyer, D. J. Magnetic Localization in Transition-Metal Nanowires. *Phys. Rev. B* **2000**, *62*, 3900–3904.

(50) Garcia, J. M.; Asenjo, A.; Velzquez, J.; Garcia, D.; Vazquez, M.; Aranda, P.; Ruiz-Hitzky, E. Magnetic Behavior of an Array of Cobalt Nanowires. *Jpn. J. Appl. Phys.* **1999**, *85*.

(51) Pirota, K.; Vazquez, M. Arrays of Electroplated Multilayered Co/Cu Nanowires with Controlled Magnetic Anisotropy. *Adv. Eng. Mater.* **2005**, *7*, 1111–1113.

(52) Rosa, W.; Vivas, L.; Pirota, K.; Asenjo, A.; Vazquez, M. Influence of Aspect Ratio and Anisotropy Distribution in Ordered CoNi Nanowire Arrays. *J. Magn. Magn. Mater.* **2012**, *324*, 3679 – 3682.

(53) Han, G. C.; Zong, B. Y.; Luo, P.; Wu, Y. H. Angular Dependence of the Coercivity and Remanence of Ferromagnetic Nanowire Arrays. *J. Appl. Phys.* **2003**, *93*.

(54) Lavin, R.; Denardin, J. C.; Escrig, J.; Altbir, D.; Cortes, A.; Gomez, H. Angular Dependence of Magnetic Properties in Ni Nanowire Arrays. *J. Appl. Phys.* **2009**, *106*.

(55) Lavin, R.; Gallardo, C.; Palma, J.; Escrig, J.; Denardin, J. Angular Dependence of the Coercivity and Remanence of Ordered Arrays of Co Nanowires. *J. Magn. Magn. Mater.* **2012**, *324*, 2360 – 2362.

(56) Vivas, L. G.; Vazquez, M.; Escrig, J.; Allende, S.; Altbir, D.; Leitao, D. C.; Araujo, J. P. Magnetic Anisotropy in CoNi Nanowire Arrays: Analytical Calculations and Experiments. *Phys. Rev. B* **2012**, *85*, 035439.

1
2
3
4
5
6
7
8
9
10
11
12
13
14
15
16
17
18
19
20
21
22
23
24
25
26
27
28
29
30
31
32
33
34
35
36
37
38
39
40
41
42
43
44
45
46
47
48
49
50
51
52
53
54
55
56
57
58
59
60

TOC GRAPHIC

Single-nanowire magnetic model

Radially Nanowires Array

$\hat{r}$

$\hat{n}$

α

Al wire

H_{axial}

$H_{transversal}$

HRSEM images of the nanowire arrays in the CNAAM structure; (a) Al wire after second anodization, (b) cross-section of the alumina layer grown on the Al wire substrate, (c) top-view of the electrodeposited nanowires in the hexagonally ordered pores of the CNAAM template and (d) higher magnification image of cross section of the electrodeposited nanowires embedded in the alumina template.
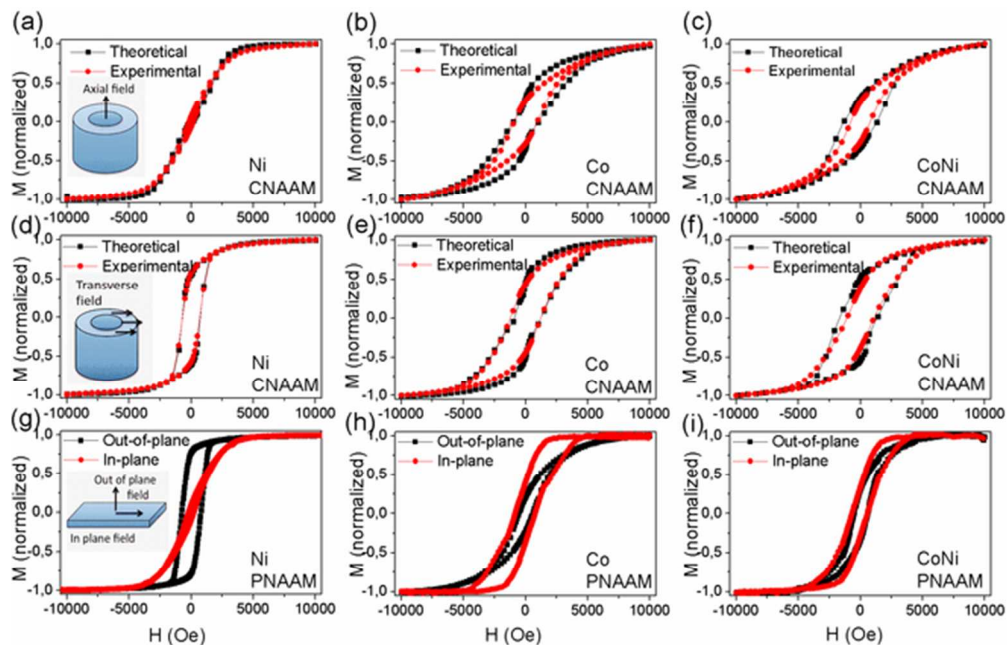
278x190mm (96 x 96 DPI)
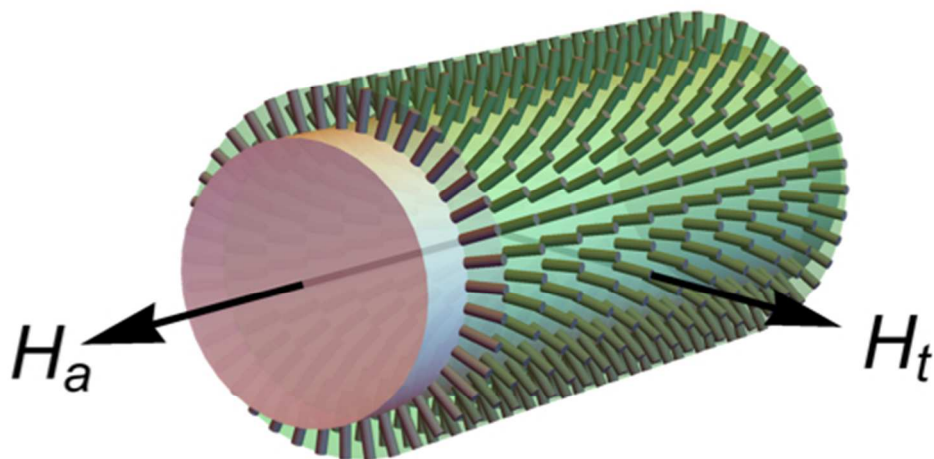
Schematic transverse view of the CNAAM filled with nanowires. Axial and transverse directions of the applied magnetic field are displayed.

99x51mm (144 x 144 DPI)
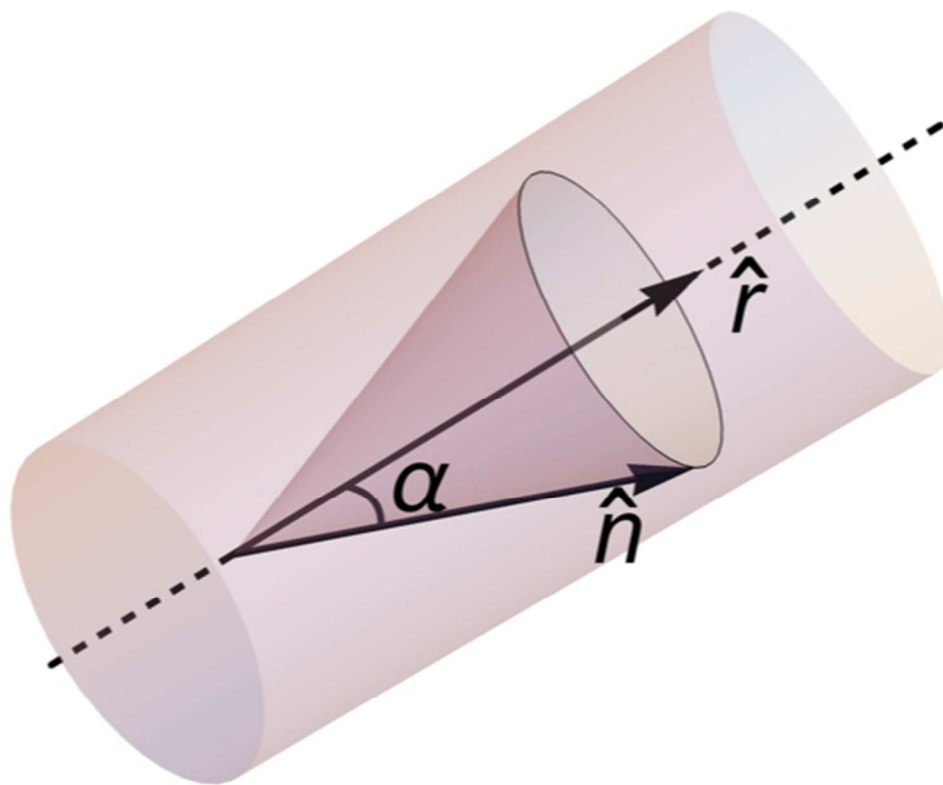
Schematic drawing of the conical anisotropy distribution in a single nanowire.

103x82mm (144 x 144 DPI)

Experimental and MC model hysteresis loops for Ni (a, d), Co (b, e) and CoNi (c, f) nanowires in a CNAAM with magnetic field applied axial and transverse with respect to the Al wire. The model used the values given in Table II. Hysteresis loops for in-plane (PNAAM) nanowires with compositions (g) Ni, (h) Co and (i) Co75Ni25.

55x36mm (300 x 300 DPI)
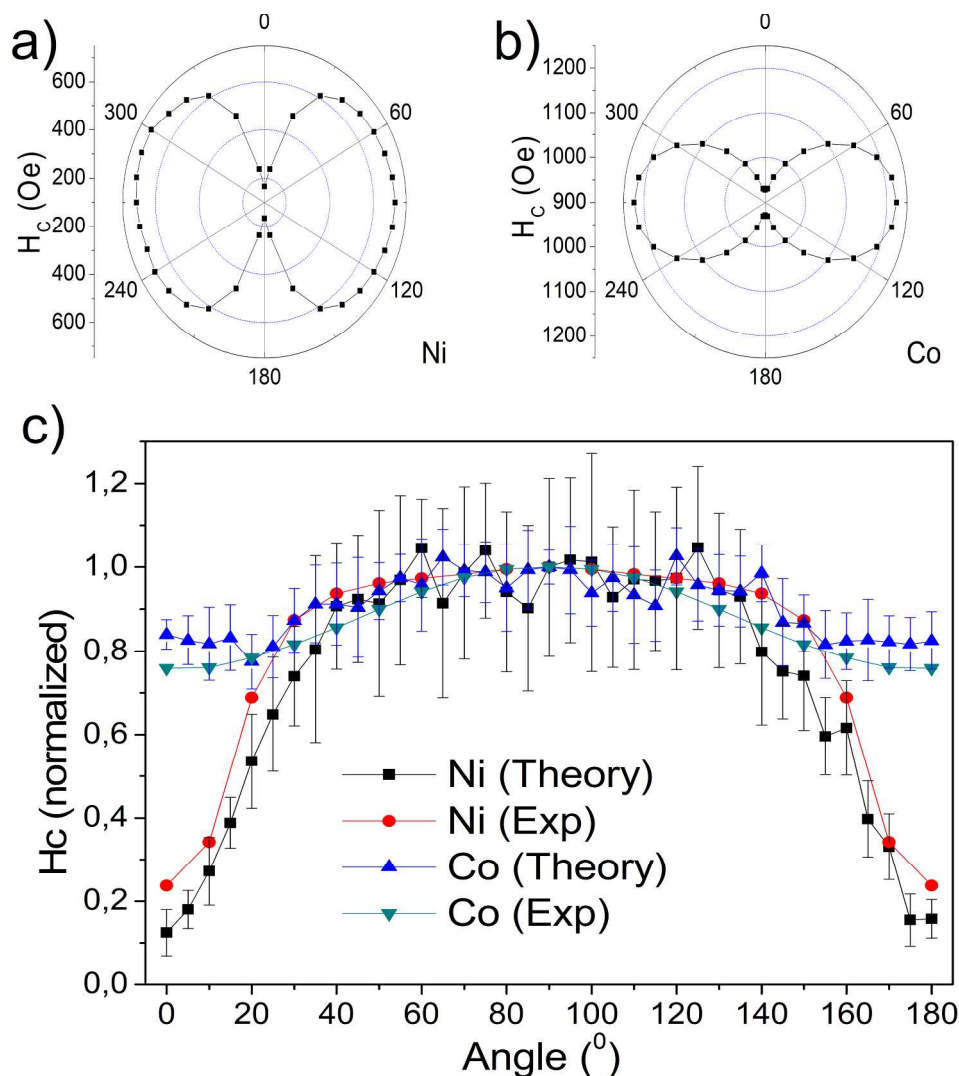
Angular dependence of the coercivity of nanowires
grown in a CNAAM with composition (a) Ni, (b) Co, shown
in polar representation. (c) Experimental and Monte Carlo
modeling results for the angular dependence of the coercive
field of Co and Ni nanowire arrays in CNAAMs.

231x244mm (300 x 300 DPI)